ChemComm

Visualization of Slide-ring Effect: A study on Movable Cross-Linking Points Using Mechanochromism

Journal:	*ChemComm*
Manuscript ID	CC-COM-12-2019-009452.R1
Article Type:	Communication

COMMUNICATION

Visualization of Slide-ring Effect: A study on Movable Cross-Linking Points Using Mechanochromism

Received 00th January 20xx,
Accepted 00th January 20xx

DOI: 10.1039/x0xx00000x

Yi Lu,[a] Daisuke Aoki,[a] Jun Sawada,[a] Takahiro Kosuge,[a] Hiromitsu Sogawa,[a] Hideyuki Otsuka,*[a] and Toshikazu Takata*[a]

To evaluate the 'slide-ring' effect in rotaxane cross-linked network, we incorporated mechanochromophores into static and rotaxane cross-linking points and compared the mechanochromisms exhibited by the obtained polymers. This novel strategy reveals a molecular-level phenomenon with visible color change as well as quantitative electron paramagnetic resonance measurements.

Rotaxane cross-linked polymers (RCPs) are highly interesting both from a fundamental scientific and from an applied industrial perspective as they exhibit significantly improved mechanical properties compared to conventional covalently cross-linked polymers (CCPs)[1]. These improved qualities are generally attributed to the unique slide-ring structures of their cross-linking points, which are considered to be movable during deformation and results in a dispersion of the applied stress. Although the macroscopic mechanical properties of various types of RCPs have been thoroughly documented,[2] molecular-level observations and evaluations of the slide-ring events still remain challenging.[3] Upon carefully inspecting small-angle neutron scattering (SANS) patterns of a cyclodextrin/poly(ethylene glycol) slide-ring gel, Shibayama and Ito *et al.* reported characteristic 'normal' butterfly patterns induced by the 'pulley effect'.[4] The same strategy was extended to small-angle X-ray scattering (SAXS) measurements,[1d,5] albeit that this technique requires highly brilliant irradiation. Soon after, atomic force microscopy (AFM) was used to obtain nanoscale insight into the role of steric and non-covalent interactions during the threading and de-threading events of single-molecule rotaxanes.[6] Nevertheless, the aforementioned approaches entail sophisticated experimental setups, which somewhat limit their universal practical applicability.

The development of mechanochromic chemistry has provided new tools to probe microscopic information via chemical reactions during the deformation of materials.[7] In particular, various mechanophores have been applied to clarify the failure mechanisms of polymers[8] and to detect minor damage to polymeric materials prior to structural disintegration, i.e., macroscopic fracture.[7c,9] These studies inspired us to attempt to visualize molecular-level events involving a combination of rotaxane and mechanochromic chemistry in RCPs.[8c,10] Very recently, De Bo *et al.* have coupled a rotaxane motif with a proximal-exo Diels-Alder adduct mechanophore and demonstrated a competing relationship between mechanochemical bond scission and slide-ring events using a combination of experimental and computational techniques.[3b] Moreover, Sagara *et al.* have developed mechanochromic fluorescent force transducers based on the slide-ring properties of rotaxanes.[11]

We realized that the methodology in the aforementioned studies could potentially be extended by employing a mechanochromophore such as diarylbibenzofuranone (DABBF). In response to mechanical force, DABBF experiences homolytic bond cleavage that generates the corresponding arylbenzofuranone (ABF) radicals, which exist in equilibrium with the dormant bonded species in air, without any side reactions.[12] The scission of the dynamic bond occurs prior to the cleavage of other typical covalent bonds and produces an easily recognizable blue color.[10a] Moreover, the generation of ABF radicals from DABBF in response to mechanical force can be quantitatively evaluated *in situ* by electron paramagnetic resonance (EPR) spectroscopy.[8a,9c]

Herein, we report the evaluation of the slide-ring effect in a novel DABBF-rotaxane-cross-linked polymer (**D-RCP**, Fig. 1a) at the molecular level using the mechanochromic behavior of the DABBF moiety. **D-RCP** was synthesized by cross-linking a polymer matrix using a DABBF-rotaxane cross-linker (**D-RC**), in which a DABBF moiety (Fig. 1b) was introduced between two *sec*-ammonium/crown ether-based rotaxane structures (Fig. 1c). The symmetric design ensures that the central DABBF motif can undergo sterically unbiased

[a] *Department of Chemical Science and Engineering, Tokyo Institute of Technology, Meguro-ku, Ookayama 2-12-1 S1-6, Tokyo, Japan.*
E-mail: otsuka@polymer.titech.ac.jp; takata.t.ab@m.titech.ac.jp
†Electronic Supplementary Information (ESI) available: [details of any supplementary information available should be included here]. See DOI: 10.1039/x0xx00000x

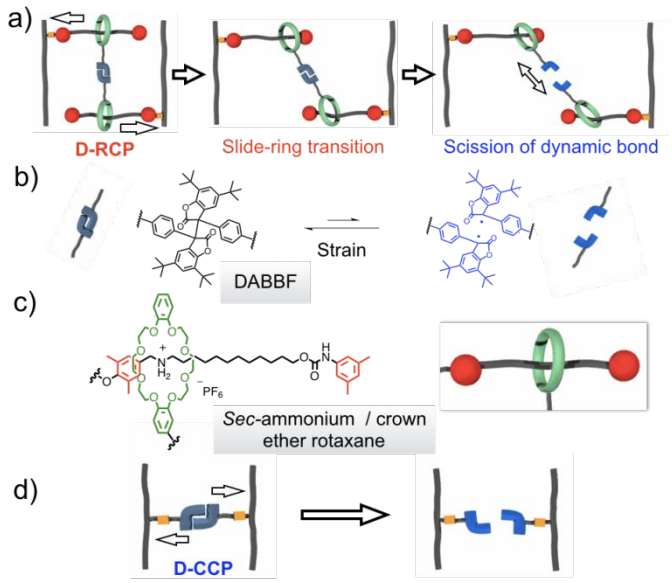

Fig. 1 Schematic illustration of the concept of this study: (a) Two-stage deformation of D-RCP, (b) mechanochromism of DABBF, (c) structure of the *sec*-ammonium/crown ether rotaxane, and (d) deformation of D-CCP.

cleavage. The dissociation energy of the hydrogen bond between the *sec*-ammonium and the crown ether of the rotaxane (< 30 kJ mol^{-1})[13] is lower than those of the dynamic covalent bonds in DABBF (85.4–104.8 kJ mol^{-1}),[10a,14] which in turn are lower than those of typical C–C bonds (e.g. in C_2H_6: ~380 kJ mol^{-1}).[15] Based on these relative bond strengths, we envisioned that the deformation of **D-RCP** upon exposure to strain would occur preferentially at the cross-linking points, and that this deformation would include two molecular-level stages (Fig. 1a). In the first stage, the rotaxane macrocycle would be pulled toward the bulky 3,5-dimethylphenyl stopper on the axle. Once the macrocycle reaches the bulky end of the axle, the dynamic bond of DABBF will be cleaved during the second stage. To demonstrate the slide-ring effect, i.e., the hierarchical cleavage, we also synthesized **D-CCP** (Fig. 1d), which is a network polymer that is cross-linked using the same concentration of DABBF motifs but does not include the slide-ring structures. The degree of dynamic bond scission due to tensile strain in both **D-CCP** and **D-RCP** was characterized and compared visually by color change and quantitatively by *in-situ* EPR measurements.

To synthesize [3]rotaxane **D-RC** (Scheme 1a), **D-CC** was coupled with DB24C8 crown ether using Steglich esterification conditions to produce **D-2MC**, which contains one macrocycle on each side of the dynamic covalent bond. The synthesized **D-2MC** was combined with two molecules of **Axle** to produce a pseudo[3]rotaxane, which was then end-capped with 3,5-dimethylphenyl isocyanate, followed by deprotection of the triisopropylsilyl ether (TIPS) groups to afford **D-RC** (for details, see the SI).

The synthetic routes to **D-CCP** and **D-RCP** are shown in Scheme 1b. Following the work of Shen *et al.*,[16] we prepared a methyl acrylate (MA)-based random copolymer modified with 3-isopropenyl-α,α-dimethylbenzyl isocyanate (TMI) as the matrix polymer (**MP**) via free radical polymerization. PMA was chosen for its moderate glass-transition temperature (T_g = 10 °C), which should permit efficient activation of the mechanochromophore[17] as well as good matrix mobility to allow the macrocycles of the rotaxanes to slide along their axles.[1c-1e] After workup, gel permeation chromatography (GPC, Fig. S1) was used to determine the molecular weight (M_n = 52 kDa) and the polydispersity (PDI = 1.87) of the obtained **MP**. The ratio of the TMI and MA moieties (m / n = 1 / 22) was determined by ^{1}H NMR spectroscopy (Fig. S3, Table S1). The IR spectrum of **MP** (Fig. S2) showed an absorption peak at 2256 cm^{-1}, indicative of the presence of isocyanate groups. The T_g of **MP** (12.9 °C) was measured by differential scanning calorimetry (DSC, Fig. S6a). Subsequently, a solvent casting method was used to obtain **D-CCP** and **D-RCP** via a dibutyltin-dilaurate (DBTDL)-catalyzed curing reaction between the isocyanate groups of **MP** and the hydroxy groups of the cross-linkers (**D-CC** and **D-RC**, respectively). After the removal of non-cross-linked reactant, **D-RCP** and **D-CCP** exhibited similar swelling properties (Table S2). Our previous work has demonstrated that short-axle *sec*-ammonium/crown ether RCPs exhibit swelling behavior similar to that of CCPs with the same cross-linking density.[1c] Therefore, we

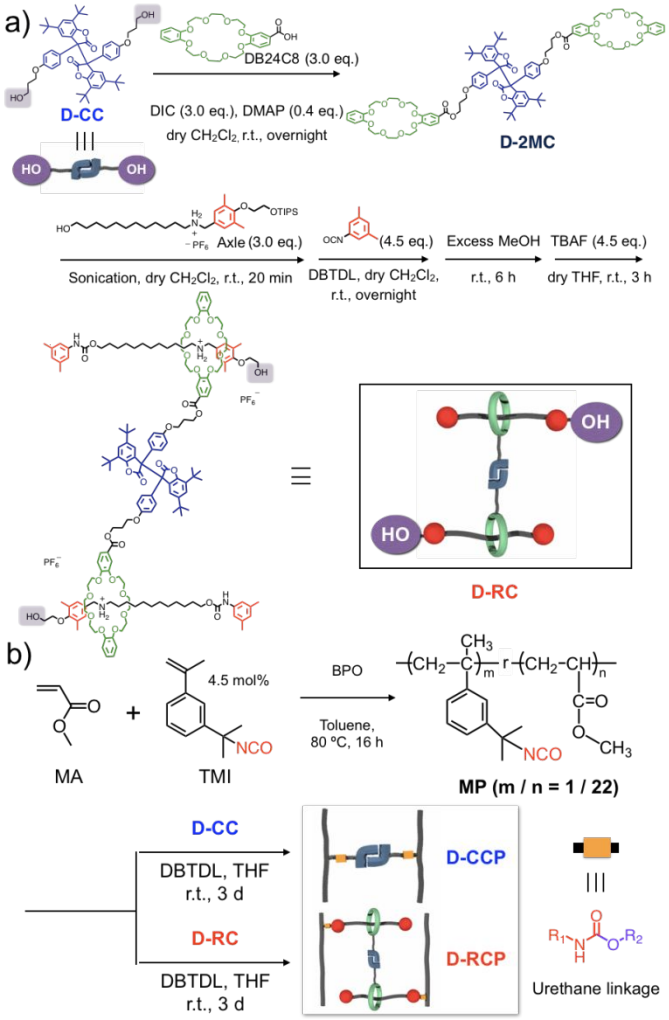

Scheme 1 Synthesis and structures of (a) DABBF-rotaxane cross linker **D-RC** and (b) cross-linked polymers **D-RCP** and **D-CCP**.

concluded that the same concentration of DABBF moieties had been successfully incorporated as cross-linking points in the network

polymers **D-RCP** and **D-CCP**. A similar impact of cross-linking upon the thermophysical properties was also confirmed by DSC. The T_gs of both **D-RCP** and **D-CCP** were observed at ~5 °C (Fig. S6b, S6c), indicating that these two samples are elastomers suitable for tensile tests.

Subsequently, dumbbell-shaped samples of **D-RCP** and **D-CCP** were prepared and subjected to tensile tests (Fig. 2a, Table S2). The corresponding stress–strain curves revealed that the Young's modulus of **D-RCP** (3.9 MPa) is lower than that of **D-CCP** (8.4 MPa) in the low strain range (0–8%). The fracture energy of D-RCP (4.4 MJ / m^3) was also lower than that of D-CCP (6.8 MJ / m^3). **D-RCP** (maximum strain: 570%) was more extensible than **D-CCP** (maximum strain: 490%).

The mechanochromic behavior of both samples was characterized visually during the tensile elongation tests (Fig. 2b; Movie S1 for **D-CCP**; Movie S2 for **D-RCP**). When no strain was applied, both samples were white films, indicating that the DABBF equilibriums of both polymers were dominated by the dormant dynamic covalent bond in the initial state. After strain had been applied, **D-CCP** underwent a dramatic white-to-blue color change; the blue color was first observed only in a small spot but eventually spread over the entire deformed domain, demonstrating the efficient cleavage of the covalently introduced DABBF moieties. On the other hand, a color

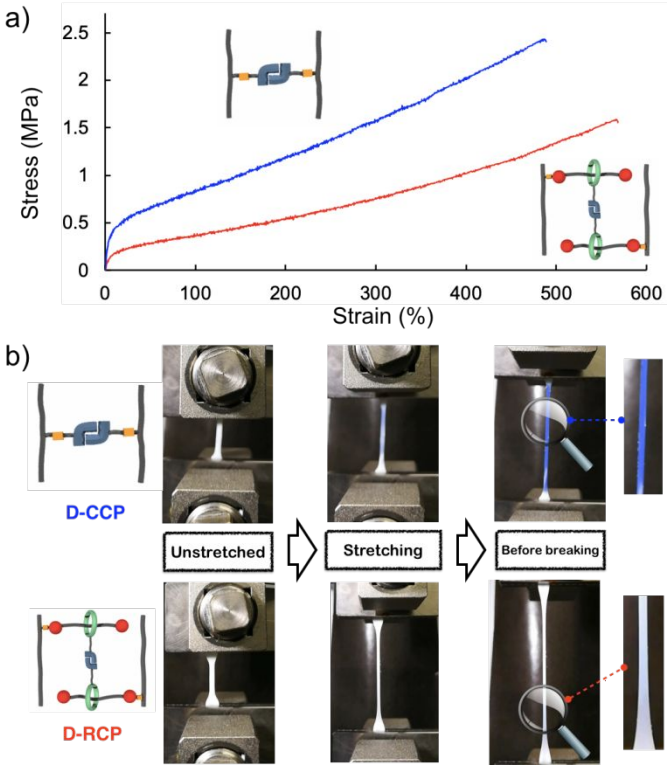

Fig. 2 Tensile tests of **D-CCP** and **D-RCP** (dumbbell-shaped samples; sample size: 12 mm × 2 mm × 0.32–0.45 mm; elongation rate: 10 mm min^{-1}). (a) Stress-strain curves. (b) Photographs during tensile elongation.

change was not observed for **D-RCP** during the early stages of deformation. Immediately before the fracture, a faint blue domain emerged. Notably, the blue color was only observed at the location where the fracture of the sample eventually occurred, which suggests a correlation between the cleavage of DABBF and the fracture of the sample. The weak mechanochromism of **D-RCP** reflects the low cleavage efficiency of mechanically linked DABBF. The low degree of cleavage could be attributed to: 1) Energy loss of the applied force due to the sliding of the ring structure of the rotaxane, which prevents an effective transfer of the mechanical force to the DABBF moiety, and 2) rapid recombination of DABBF, which is facilitated by the high mobility of the rotaxane moieties at the cross-linking points.[8b] Because the dynamic bonds of DABBF served as sacrificial bonds to contribute toughness, the insufficient cleavage of these bonds in **D-RCP** resulted in a lower Young's modulus as well as fracture energy, and a higher strain, compared to **D-CCP**.

To quantify this mechanochromism, we prepared long strips of the samples and carried out *in-situ* EPR measurements during uniaxial tensile elongation (Fig. 3). In the unstrained state, the amount of dissociated DABBF in **D-RCP** (0.002%) was approximately the same as

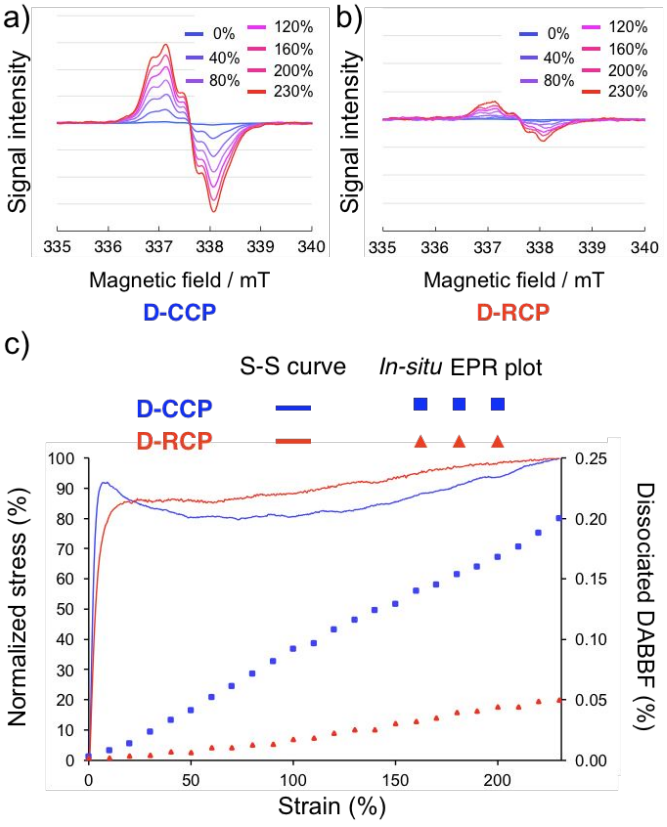

Fig. 3. EPR spectra of (a) **D-CCP** and (b) **D-RCP** with increasing strain (0, 40, 80, 120, 160, 200, and 230 %). The intensity was normalized by the volume, assuming a Poisson ratio of 0.5. (c) *In-situ* EPR measurements during elongation: Stress–strain curves obtained using long strip samples; the stress was normalized and is given as a percentage of the maximum stress, while the ratio of dissociated DABBF in both samples is shown as a function of the strain.

that in **D-CCP** (0.003%). During tensile elongation, the EPR intensities were recorded in increments of 10% increase in strain (Fig. 3a, 3b); the dissociation of DABBF increased in a linear fashion with increasing strain (Fig. 3c).[9c] Remarkably, the dissociation rate for **D-**

RCP was about four times lower than that of **D-CCP**, which is in agreement with our visual observations. Both measurements ended at 230% strain, where 0.049% and 0.200% of the DABBF was dissociated in **D-RCP** and **D-CCP**, respectively.

The *in-situ* EPR measurements revealed a noticeable difference between the dissociation rates of DABBF in **D-RCP** and **D-CCP**. As expected, the slide-ring event in **D-RCP** acts as a buffer for the applied strain, thus preventing the mechanical force from being effectively transferred to the DABBF mechanochromophores. Moreover, the linear increase in the amount of ABF radicals in both cases suggests a shift in the equilibrium between the cleavage of DABBF and the recombination of ABF during the deformation. Due to the high mobility of the rotaxane moieties connected to DABBF, the recombination of the generated ABF radicals in **D-RCP** was faster than that in **D-CCP**. Consequently, a lower DABBF activation rate was observed for **D-RCP**.

In summary, we prepared a novel network polymer **D-RCP**, in which DABBF moieties connect rotaxane cross-linking points, to visualize and quantitatively characterize the slide-ring effect during tensile elongation via the mechanochromic properties of DABBF. Together with the qualitative visual indicator (color change), which is a simple and intuitive method that is particularly attractive for practical applications, a quantitative analysis of the mechanochromism was accomplished by *in-situ* EPR measurements that demonstrated the role of the slide-ring structure in the deformation of this RCP. As the DABBF units are synthetically linked to the functional rotaxane structures, this approach allowed the investigation of the microscopic events during deformation. To the best of our knowledge, this is the first report in which mechanochromism is used to gather *in-situ* microscopic information on a bulk system in order to understand the deformation mechanism of an RCP. We expect that this method can also be used to evaluate other emerging materials and shed light on hitherto unclear or controversial failure mechanisms. Significantly, this method allows the qualitative visualization of molecular-level events using the naked eye, as well as their quantification using EPR spectroscopy.

Conflicts of interest

There are no conflicts to declare.

Notes and references

1 (*a*) Y. Okumura and K. Ito, *Adv. Mater.*, 2002, **13**, 485–487; (*b*) T. Arai, K. Jang, Y. Koyama, S. Asai and T. Takata, *Chem. Eur. J.*, 2013, **19**, 5917–5923; (*c*) J. Sawada, D. Aoki, M. Kuzume, K. Nakazono, H. Otsuka and T. Takata, *Polym. Chem.*, 2017, **8**, 1878–1881; (*d*) A. Bin Imran, K. Esaki, H. Gotoh, T. Seki, K. Ito, Y. Sakai and Y. Takeoka, *Nat. Commun.*, 2014, **5**, 1–8; (*e*) J. Sawada, D. Aoki, S. Uchida, H. Otsuka and T. Takata, *ACS Macro Lett.*, 2015, **4**, 598–601; (*f*) C. Gong and H. W. Gibson, *J. Am. Chem. Soc.*, 1997, **119**, 8585–8591.

2 (*a*) K. Kato, T. Yasuda and K. Ito, *Macromolecules*, 2013, **46**, 310–316; (*b*) Y. Takashima, Y. Hayashi, M. Osaki, F. Kaneko, H. Yamaguchi and A. Harada, *Macromolecules*, 2018, **51**, 4688–4693; (*c*) S. Ikejiri, Y. Takashima, M. Osaki, H. Yamaguchi and A. Harada, *J. Am. Chem. Soc.*, 2018, **140**, 17308–17315.

3 (*a*) G. De Bo, *Chem. Sci.*, 2017, **9**, 15–21; (*b*) M. Zhang and G. De Bo, *J. Am. Chem. Soc.*, 2018, **140**, 12724–12727.

4 (*a*) T. Karino, Y. Okumura, K. Ito and M. Shibayama, *Macromolecules*, 2004, **37**, 6177–6182; (*b*) T. Karino, Y. Okumura, C. Zhao, T. Kataoka, K. Ito and M. Shibayama, *Macromolecules*, 2005, **38**, 6161–6167.

5 Y. Shinohara, K. Kayashima, Y. Okumura, C. Zhao, K. Ito and Y. Amemiya, *Macromolecules*, 2006, **39**, 7386–7391.

6 (*a*) B. Brough, B. H. Northrop, J. J. Schmidt, H. R. Tseng, K. N. Houk, J. F. Stoddart and C. M. Ho, *Proc. Natl. Acad. Sci.*, 2006, **103**, 8583–8588; (*b*) P. Lussis, T. Svaldo-Lanero, A. Bertocco, C. A. Fustin, D. A. Leigh and A. S. Duwez, *Nat. Nanotechnol.*, 2011, **6**, 553–557.

7 (*a*) Z. Wang, Z. Ma, Y. Wang, Z. Xu, Y. Luo, Y. Wei and X. Jia, *Adv. Mater.*, 2015, **27**, 6469–6474; (*b*) F. Verstraeten, R. Göstl and R. P. Sijbesma, *Chem. Commun.*, 2016, **52**, 8608–8611; (*c*) R. Göstl and R. P. Sijbesma, *Chem. Sci.*, 2016, **7**, 370–375; (*d*) C. Calvino, L. Neumann, C. Weder and S. Schrettl, *J. Polym. Sci. Part A Polym. Chem.*, 2017, **55**, 640–652; (*e*) H. Zhang, X. Li, Y. Lin, F. Gao, Z. Tang, P. Su, W. Zhang, Y. Xu, W. Weng and R. Boulatov, *Nat. Commun.*, 2017, **8**, 1147; (*f*) Y. Chen, A. J. H. Spiering, S. Karthikeyan, G. W. M. Peters, E. W. Meijer and R. P. Sijbesma, *Nat. Chem.*, 2012, **4**, 559–562.

8 (*a*) K. Imato, T. Kanehara, S. Nojima, T. Ohishi, Y. Higaki, A. Takahara and H. Otsuka, *Chem. Commun.*, 2016, **52**, 10482–10485; (*b*) T. Kosuge, K. Imato, R. Goseki, H. Otsuka, *Macromolecules*, 2016, **49**, 5903–5911; (*c*) D. A. Davis, A. Hamilton, J. Yang, L. D. Cremar, D. Van Gough, S. L. Potisek, M. T. Ong, P. V. Braun, T. J. Martínez, S. R. White, J. S. Moore and N. R. Sottos, *Nature*, 2009, **459**, 68–72; (*d*) S. Jiang, L. Zhang, T. Xie, Y. Lin, H. Zhang, Y. Xu, W. Weng and L. Dai, *ACS Macro Lett.*, 2013, **2**, 705–709; (*e*) M. B. Larsen and A. J. Boydston, *J. Am. Chem. Soc.*, 2013, **135**, 8189–8192.

9 (*a*) N. Bruns, K. Pustelny, L. M. Bergeron, T. A. Whitehead and D. S. Clark, *Angew. Chem. Int. Ed.*, 2009, **48**, 5666–5669; (*b*) D. W. R. Balkenende, S. Coulibaly, S. Balog, Y. C. Simon, G. L. Fiore and C. Weder, *J. Am. Chem. Soc.*, 2014, **136**, 10493–10498; (*c*) K. Imato, T. Kanehara, T. Ohishi, M. Nishihara, H. Yajima, M. Ito, A. Takahara and H. Otsuka, *ACS Macro Lett.*, 2015, **4**, 1307–1311.

10 (*a*) K. Imato, A. Irie, T. Kosuge, T. Ohishi, M. Nishihara, A. Takahara and H. Otsuka, *Angew. Chem. Int. Ed.*, 2015, **54**, 6168–6172; (*b*) Y. Lin, M. H. Barbee, C. C. Chang and S. L. Craig, *J. Am. Chem. Soc.*, 2018, **140**, 15969–15975.

11 (*a*) Y. Sagara, M. Karman, A. Seki, M. Pannipara, N. Tamaoki and C. Weder, *ACS Cent. Sci.*, 2019, **5**, 874–881; (*b*) Y. Sagara, M. Karman, E. Verde-Sesto, K. Matsuo, Y. Kim, N. Tamaoki and C. Weder, *J. Am. Chem. Soc.*, 2018, **140**, 1584–1587.

12 H. G. Korth, *Angew. Chem. Int. Ed.*, 2007, **46**, 5274–5276.

13 (*a*) P. R. Ashton, P. J. Campbell, P. T. Glink, D. Philp, N. Spencer, J. F. Stoddart, E. J. T. Chrystal, S. Menzer, D. J. Williams and P. A. Tasker, *Angew. Chem. Int. Ed.,* 1995, **34**, 1865–1869; (*b*) T. Steiner, *Angew. Chem. Int. Ed.*, 2002, **41**, 48–76.

14 M. Frenette, C. Aliaga, E. Font-Sanchis and J. C. Scaiano, *Org. Lett.*, 2004, **6**, 2579–2582.

15 S. J. Blanksby and G. B. Ellison, *Acc. Chem. Res.*, 2003, **36**, 255–263.

16 K. H. Wu, L. F. Feng, X. P. Gu, C. L. Zhang, S. Shen, *Ind. Eng. Chem. Res.*, 2018, **57**, 946–953.

17 T. Kosuge, K. Imato, R. Goseki, H. Otsuka, *Macromolecules*, 2016, **49**, 5903–5911.